NMR and Microelectrode Studies of Hydrodynamics and Kinetics in Biofilms

Zbigniew Lewandowski,*,† Stephen A. Altobelli,‡ and Eiichi Fukushima‡

National Science Foundation Research Center for Interfacial Microbial Process Engineering, Montana State University, Bozeman, Montana 59717, and Lovelace Medical Foundation, 2425 Ridgecrest Drive SE, Albuquerque, New Mexico 87108

Profiles of flow velocity and dissolved oxygen concentration were studied by NMR and microelectrodes near mixed population biofilms growing on polycarbonate substratum. The profile of dissolved oxygen concentration within the diffusion boundary layer and profiles of flow velocity within the hydrodynamic boundary layer can be described by exponential equations.

Introduction

In aquatic environments, bacteria attach to surfaces (substratum) where they reproduce and excrete extracellular polymers to form viscoelastic layers called biofilms. Biofilms use chemical compounds dissolved in the bulk solution as substrates for growth. Substrate conversion rate in biofilms is limited by mass transfer. The mass transfer to and from biofilms occurs through the biofilm/bulk water interface. Thus, the local chemical environment and flow conditions influence the extent of biofilm growth. The chemical environment is modified near biofilms in proportion to the biofilm substrate conversion rate, and the local hydrodynamics is altered by the irregular growth of the film. Because of these complications, approaches to understanding local properties of biofilm systems are largely experimental. Techniques for measuring biofilm reaction kinetics have depended on two types of analyses: (1) chemical analysis of bulk water and (2) local chemical and physical measurements inside the biofilm using microsensors.

Chemical analysis of bulk water delivers information about average biofilm activity. In particular, a mass balance based on chemical analysis of the influent and effluent of a biofilm reactor can be performed. The calculated substrate conversion rate can be referred to a unit of reactor's surface. Such a calculation would reflect average properties of the system, but has serious limitations when predicting local chemistry near biofilms.

The substrate concentration varies vertically within the biofilm system, forming concentration profiles, but the biofilm is usually quite thin relative to the lateral dimensions, limiting the space needed for intrafilm instrumentation measurements. Microsensors, usually microelectrodes which are sensitive to specific ions, compounds, or dissolved gases, are constructed with tip diameters of a few micrometers and are driven across the biofilm by motorized micromanipulators (Whalen et al., 1969; Bungay et al., 1969; Revsbech and Jorgensen, 1986; Riethues et al., 1986; Baumgartl, 1987). The measurements are conducted in intervals from a few to a few hundred micrometers. Electrodes with tip diameters of 10 micrometers or less are required because the tip should penetrate the biofilm without physical damage to its structure. Larger electrodes produce dents in the biofilm, allowing bulk water to penetrate and influence the measurement. Some measurements, which rely on mass transfer between the environment and the sensor (e.g., amperometry), actually consume the substrate during measurement with a rate that is proportional to sensor surface. A probe with significant surface area may substantially interfere with the system.

Each chemical that is consumed or produced in the film forms a separate concentration profile. The substrate is consumed by the biofilm growing on the surface and at the same time is supplied from the bulk water, but other compounds which are produced in the biofilms form reversed profiles, i.e., the compound is supplied by the biofilm and "consumed" by the bulk water by dilution. Each point of a concentration profile reflects a local equilibrium between consumption and supply. The shape of the profile is influenced by all factors influencing the biofilm system (hydrodynamics, temperature, presence or absence of biocides, reaction with substratum, etc.). The profiles must be measured in situ, because transferring biofilm to another environment changes the profiles and the results no longer reflect the original conditions.

Conventional analysis of biofilm reactors depends on mass balances because concentration profiles, derived from microsensors, do not directly provide the necessary information. A procedure of kinetic parameters calculation from substrate concentration profiles was presented by Lewandowski et al. (1991). This procedure is, however, limited to stagnant water where the substrate concentration profile across the diffusion boundary layer is linear. For flowing water, this part of the profile becomes nonlinear, which complicates the analysis. The spatial distribution of the concentration is also involved since the results of microsensor measurement are site specific.

Hydrodynamics influences biofilm accumulation in many ways. During the initial events of biofilm formation, it controls the transport of microorganisms to the surface (Duddridge et al., 1982). After the film is formed, hydrodynamics controls the transport of substrate to the biofilm. The biofilm accumulation rate is the net result of microbial attachment, detachment, and growth rates. Attachment is defined as microbial transport and adsorption onto the surface, detachment is microbial desorption from the surface, and growth is microbial multiplication at the surface, and all three are influenced by hydrodynamics. Attachment rate is controlled by transport of microorganisms with flowing water. Detachment rate is influenced by erosion, which directly depends on

*Author to whom all correspondence should be addressed.
† Montana State University.
‡ Lovelace Medical Foundation.

8756-7938/93/3009-0040$04.00/0

the shear stress. Growth rate depends on substrate transport rate, which is a function of turbulence.

The biofilm formation changes the surface and modifies the hydrodynamics of the system. This process seems to be particularly effective once the biofilm thickness becomes comparable to the thickness of the hydrodynamic boundary layer. Picolloglou et al. (1980) observed a considerable increase in frictional resistance after film thickness reached a value approximately equal to the calculated thickness of the hydrodynamic boundary layer for a clean surface. Biofilm accumulation at surfaces is an autocatalytic process. Initial colonization of surface increases surface roughness and promotes further formation of biofilm. Bouwer (1987) points out that increased surface roughness due to biofilm formation can influence particle transport rate and biofilm attachment rate by (1) increasing convective mass transport near the surface, (2) providing shelter from shear forces, and (3) increasing surface area for attachment. A study by Siegriest and Gujer (1985) showed that biofilm roughness can increase eddy diffusion and the external mass transfer rate into the biofilm. Cunningham (1989) postulates that as a biofilm surface element extends outward through the boundary layer it is subjected to increased convective transport, which contributes not only to accumulation but also to an increased shear stress which contributes to erosion (Rittmann, 1982). Lewandowski and Walser (1991), using a rotating disc reactor, demonstrated that biofilm thickness reaches a maximum within the transition zone between the laminar and turbulent flow. It was postulated that for laminar flow the biofilm thickness was limited by transport of substrate and for turbulent flow by erosion due to increased shear stress.

Fluid mechanics typically describes conditions near rigid surfaces, but a biofilm consists mainly of viscoelastic biopolymers and its surface is soft and sometimes filamentous. In fact, the nature of the surface can be a function of the hydrodynamics; for example soft, filamentous biofilm surfaces can be rougher for low flow velocities than for higher velocities. With increasing fluid flow velocities, the filaments may yield to the flow, resulting in a smoother surface. There is no theoretical treatment which could be directly applied to describe the flow near such surfaces.

The existing descriptions of relations between hydrodynamics and kinetics in biofilm systems are qualitative. Three zones of diffusion near the biofilm surface have been distinguished by Revsbech and Jorgensen (1986): (1) the eddy diffusion zone; (2) the transition zone; and (3) the molecular diffusion zone. This last zone, the molecular diffusion zone, is adjacent to the biofilm/liquid interface and extends through the entire biofilm layer. The changes in diffusivity close to the biofilm surface are attributable entirely to changes in hydraulic conditions in this region.

In this article, profiles of substrate concentration and flow velocity in the diffusion boundary layer are measured. These two profiles are related because hydrodynamics is mainly responsible for the transport of dissolved oxygen to the biofilm. Two techniques are described which can be applied to investigate hydrodynamics and kinetics in biofilm systems: microelectrode concentration measurements of chemical constituents across the biofilm systems and nuclear magnetic resonance imaging (NMRI) measurements of the flow velocity profiles near biofilms. Both techniques provide a unique insight into the near-biofilm environment.

Dissolved Oxygen Concentration Profiles

The dissolved oxygen is consumed by the biofilm in the respiration process. There is no oxygen consumption in bulk water. Consequently, the dissolved oxygen concentration decreases near the biofilm surface. Each point of the dissolved oxygen concentration profile reflects an equilibrium between the rate of dissolved oxygen consumption by the biofilm and the dissolved oxygen transport rate from the bulk solution. If the dissolved oxygen transport across the boundary layer is much faster than the consumption, there is no concentration gradient near the biofilm and the system is rate-limited. If the consumption rate exceeds the dissolved oxygen transport rate across the boundary layer, then there is a concentration gradient near the biofilm and the system is diffusion-limited. Diffusion-limited reactions are slow because diffusion coefficients in liquids are small.

The transport of substrate in moving liquid is governed by two different mechanisms: first, molecular diffusion as a result of concentration gradient; and second, convection, where substrate particles are entrained by the moving liquid and are transported with it. Transport of oxygen to the biofilm interface is due to the combination of these processes. In stagnant water, transport of dissolved oxygen would be almost entirely due to molecular diffusion, neglecting any contribution from natural convection. When the water starts to flow, convection exceeds diffusion. Transport by diffusion is so slow that, even for low flow velocities, convection exceeds molecular diffusion (Levich, 1962). The faster the flow the more intense the convection. The flow velocity, however, forms gradients near surfaces because of viscosity. This changes the intensity of convection across the system. Convection is strongest in the bulk solution and decreases toward the biofilm along with the flow velocity. Consequently, the dissolved oxygen profile is not linear; the concentration gradient depends on the flow velocity profile and convection decreases. The dissolved oxygen concentration gradient is a maximum at the biofilm surface, where the flow velocity is a minimum, turbulence is absent, and transport is entirely due to molecular diffusion.

In order to measure the oxygen concentration profile, a microelectrode was made of a 0.1-mm high-purity (99.99%) platinum wire, with one end etched electrochemically in KCN to a diameter of about 2 μm. The wire was rinsed with concentrated HCl and ethanol and covered with soda-lime glass. The tip of the platinum wire was exposed by grinding on a rotating diamond wheel and was subsequently etched in KCN to yield a recess of about 10 μm. Half of this recess was filled with gold by electrochemical plating. The operation was performed under a microscope with a TV camera and observed on a video screen. The tip of the electrode was then covered with a polymer (TePeX) serving as the oxygen-permeable membrane. The measuring setup consisted of a picoammeter and a polarizing voltage source. The microelectrode was polarized to 800 mV against a silver/silver chloride reference electrode. The current in the circuit, in the range of picoamperes, is proportional to the concentration of dissolved oxygen. The electrode was calibrated in water by aeration and subsequent purging with pure nitrogen. The microelectrode was mounted on a micromanipulator and moved across the biofilm in predetermined increments. The current was measured at each position and compared with the calibration curve to yield the dissolved oxygen concentration.

Figure 1 is the dissolved oxygen profile across a biofilm system. The biofilm was an undefined, mixed population

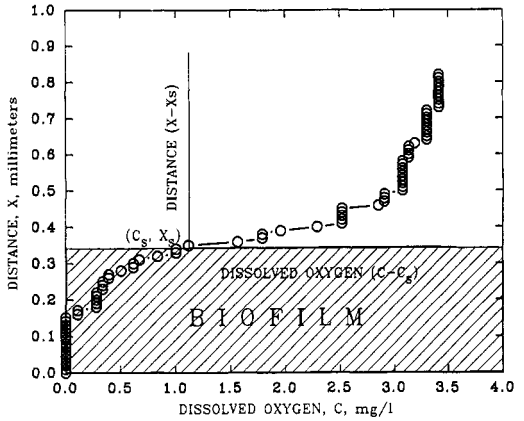

Figure 1. Dissolved oxygen concentration profile in a biofilm system.

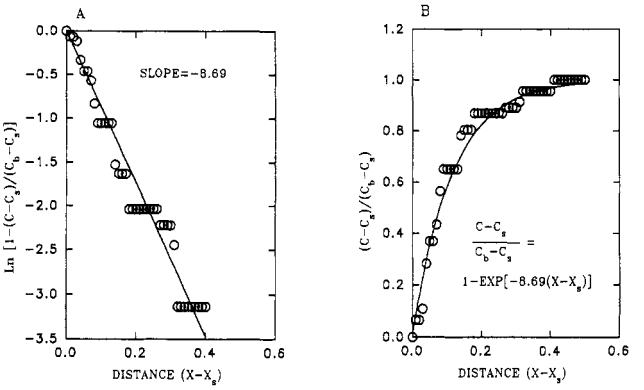

Figure 2. (A) Dissolved oxygen concentration profile from Figure 1 plotted on semi-log paper. (B) Fit of Figure 2A (—) shown in relation to the measurements (O).

growing on a polycarbonate, continuous flow, flat-plate reactor, with an average flow velocity of 3.2 cm/s. The substrate was glucose and mineral salts. The profile consists of two parts, divided by the biofilm surface. Major differences between these parts are caused by the absence of substrate uptake above the biofilm surface and of water flow below the biofilm surface. The diffusivity differences and substrate utilization in the biofilm lead to a discontinuity in the substrate concentration profile at the biofilm surface. This discontinuity arises because the mass transfer of substrate in the fluid and in the biofilm is governed by different equations tied together by the requirement that the substrate flux at the water/film interface be continuous at steady state.

The following procedure is proposed to describe the shape of the profile above the biofilm surface. First, the biofilm/water interface is located at the inflection point of the profile. A new system of coordinates (concentration, distance) was set with the origin at the biofilm surface. The shape of the profile above the biofilm surface can be described empirically in this new system of coordinates by an exponential function:

$$\frac{C - C_s}{C_b - C_s} = 1 - \exp[-B(X - X_s)] \qquad (1)$$

where C is the local substrate concentration, C_s is the substrate concentration at the biofilm surface, C_b is the bulk substrate concentration, B is an experimental coefficient, X_s is the distance from the substratum to the biofilm surface (biofilm depth), and $(X - X_s)$ is distance in the new system of coordinates. This equation can be linearized to conveniently calculate the coefficient B from experimental data:

$$\ln\left(1 - \frac{C - C_s}{C_b - C_s}\right) = -B(X - X_s) \qquad (2)$$

Coefficient B calculated as the slope of Figure 2A is -8.69. The fit of eq 2 with B = -8.69 is shown in Figure 2B.

NMR Imaging Experiments

A versatile set of noninvasive techniques using nuclear magnetic resonance (NMR) has been developed to study chemical and physical properties of small samples (see Abragam, 1961) and to allow spatial mapping, or imaging, of larger systems. Morris (1986) provides detailed descriptions of current NMR imaging methods.

Most NMR imaging (and all of the imaging described in this paper) deals with protons (^{1}H) in the liquid state. While many physical parameters of liquids may be imaged, proton concentration and velocity are emphasized here. Concentration images show where fluid is within the imaging volume; given knowledge of system boundaries, the amount of fluid displaced by an intruding solid phase may also be determined by subtraction (see Majors et al., 1989, and Altobelli et al., 1991). Velocity images provide maps of selected velocity components.

NMR experiments are performed in a strong, uniform, static magnetic field. Radio frequency (rf) magnetic fields are then applied to the sample to elicit the NMR signal, and spatially linear magnetic field gradients are superposed on the static field to encode position and velocity information into the NMR signal. Since the NMR signal arises from a rotating vector, it is convenient to simultaneously acquire two components in phase quadrature and treat the signal as complex numbers (Fukushima and Roeder, 1981).

Proton NMRI measurements were performed at 80.34 MHz on a Nalorac Quest 4300 spectrometer/imager system with an Oxford superconducting magnet (1.89 T, 31 cm horizontal bore) and a 10 cm diameter rf probe. The imaging region is limited by the magnet to a spherical volume of diameter approximately 8 cm.

The polycarbonate reactor used in this experiment had a thin rectangular chamber with a row of four round posts near the inlet end and three more posts downstream to disturb the flow. We added a paramagnetic gadolinium solution (Magnevist, Berlex Laboratories, Inc., Wayne, NJ) to the nutrient solution to reduce the spin-lattice relaxation time. Earlier, we determined that 1% Magnevist solution did not affect the growth rate of a mixed population of microorganisms, so that the 0.1% concentration used during the experiment was benign. The reactor was inoculated with activated sludge from a municipal waste water treatment plant. The biofilm was fed with a mixture of glucose and yeast extract. For details, see Lewandowski et al. (1991).

The NMR imaging described here is two-dimensional, i.e., a slice through the system is selected and parameters of interest are imaged in that slice. In two-dimensional imaging, a signal (N_r complex points) is acquired for each of N_{pe} values of a stepped gradient (the "phase-encoding" gradient). Typical values of N_r and N_{pe} are 256 and 128. Images are calculated from the acquired data set by two-dimensional Fourier transformations. For the aqueous fluid used in these experiments, a delay of ca. 1 s is used between successive repetitions, so that acquisition of an image by this technique requires steady conditions for several minutes. In this study, four or eight complete acquisition cycles were averaged; total imaging times were approximately 8–16 min.

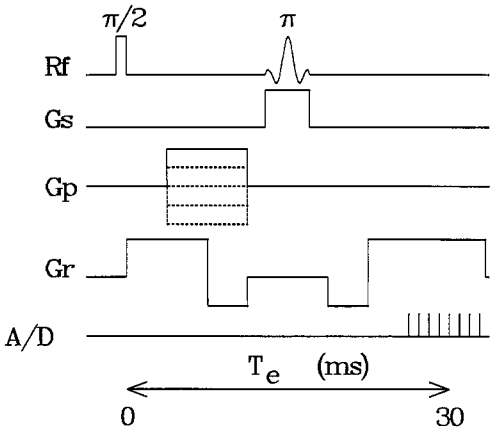

Figure 3. Timing diagram of an NMRI velocity measurement sequence. Successive lines show the timing of radio frequency, magnetic field gradients, and the analog to digital conversion pulses. G_s = slice encode, G_{pe} = phase encode, and G_r = read-out. The velocity sensitizing occurs during the slice encoding on the second line, so that this experiment measures only the velocity in the main flow direction.

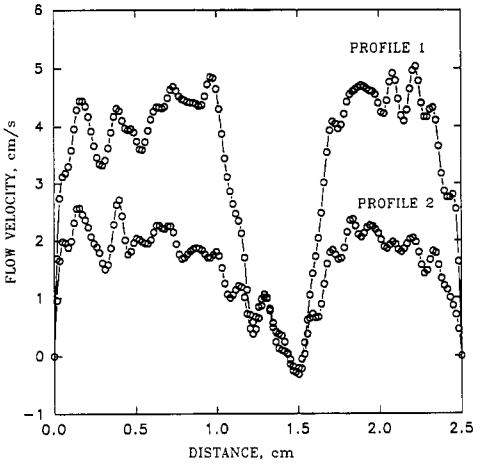

Figure 4. Two velocity profiles perpendicular to the flow direction and averaged over the thickness of the cell. A column of biofilm spanned the thickness of the channel near the center of the velocity profile in which the water is stagnant and its velocity is near zero. For profile 1, the average velocity was 4.6 cm/s; for profile 2, the average velocity was 2.2 cm/s.

In addition to the usual concentration images, it is possible to use NMR to acquire information about hydrodynamic parameters of flowing systems, as reviewed recently by Caprihan and Fukushima (1990). In particular, it is now possible to obtain detailed velocity images of steady flows in 2-D, and there have even been exploratory studies of 3-D flows and nonsteady flows. Velocity images provide maps of selected velocity components. This is accomplished by making the phase increment of the magnetization in each voxel correspond to a selected velocity component. Thus, the experimental procedure for NMR is to make measurements with the velocity-sensitizing gradient in one direction and then repeat with the gradient rotated to another direction orthogonal to the first.

Streamwise and Cross-Stream Velocity Components. One NMR experiment in this study is a dual-echo method (see Majors et al. (1990) and Lewandowski et al. (1991)), which provides images of the distribution of two orthogonal average velocity components. Images show the reactor from above, and the velocity components measured represent averages over the 2-mm thickness. These images were used to map the overall flow field before and after biofilm growth.

Streamwise Velocity Measurement at Selected Cross Sections. Another imaging sequence used is shown as a timing diagram in Figure 3. The top line of the figure shows the applied radio frequency pulses which, in conjunction with the selection gradient G_s shown below it, select a slice and produce a spin echo at time T_e (30 ms). The third line shows the timing of the stepped phase-encoding gradient G_{pe}, and the fourth line shows the velocity-compensated "read-out" gradient G_r. The fifth line of the figure indicates that signal acquisition captures the spin-echo signal. This sequence measures velocity through the slice (Cho et al., 1986).

Interpretation of the Velocity Distribution Profiles near the Biofilm. The dual-echo experiment was used to locate a section of the bioreactor in which the biofilm covered the boundary of the channel and also formed a column spanning the channel thickness. Streamwise velocity component measurements were made at this cross section. Transverse velocity profiles through the biofilm column were selected from measurements made at two flow rates, as shown in Figure 4. The figure shows the streamwise velocity component in the polycarbonate reactor as a function of the transverse dimension. Velocity was measured at points in a cross section of the reactor on a grid approximately 20 × 100. The profiles shown were selected from this grid along the horizontal center line. The side walls of the reactor define the edges of the plot, labeled 0 and 2.5 cm, and the boundary layer character of the flow near these walls is evident. A column of biomass spanned the vertical dimension of the reactor between 1.0 and 1.5 cm, where the measured velocity was near zero. In the vertical (thin) dimension the velocity varied smoothly from zero at the top and bottom walls to a maximum near the center-line profile shown. The flow velocity distribution near the biofilm surface can be described by an exponential function:

$$\frac{\nu}{\nu_b} = 1 - \exp(-AX) \tag{3}$$

where ν is the measured flow velocity, ν_b is the average, unobstructed flow velocity, and X is the distance measured from the biofilm surface. The results of fitting this equation to the measurements are shown in Figures 5 and 6 for the first and second velocity profiles of Figure 4, respectively. The significance of the small variations in the velocity between the biomass column and the side wall boundary layers is not known. In this context it should be recalled that the upstream conditions are far from uniform because of the biomass and the vertical posts.

Discussion

The flux, J, of substrate through the diffusion layer is

$$J = D\frac{dC}{dX} \tag{4}$$

Equation 4 is straightforward to use only if the concentration profile is linear and the derivative (dC/dX) is constant. If the concentration profile is nonlinear, then the derivative must be obtained analytically or graphically for the points of interest. To calculate the substrate transport to the biofilm, the derivative (dC/dX) is evaluated at the biofilm surface. From eq 1, the first derivative of concentration versus distance at the biofilm surface is

$$\left(\frac{dC}{dX}\right)_{(X-X_s)=0} = B(C_b - C_s) \tag{5}$$

From eqs 4 and 5, the flux of dissolved oxygen into the

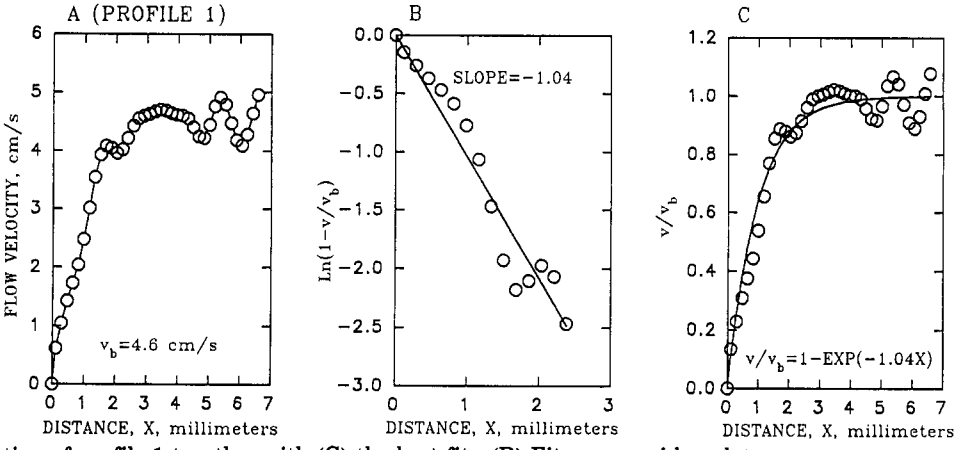

Figure 5. (A) Portion of profile 1 together with (C) the best fit. (B) Fit on a semi-log plot.

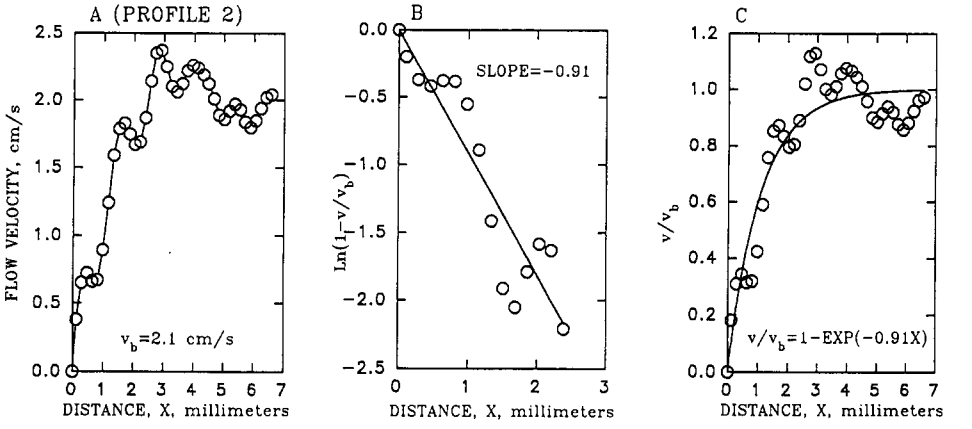

Figure 6. (A) Portion of profile 2 together with (C) its best fit. (B) Fit on a semi-log plot.

biofilm for a known diffusivity of substrate through water is

$$J = DB(C_b - C_s) \tag{6}$$

The flux of substrate into the biofilm multiplied by the surface area is equal to the substrate consumption rate:

$$R = FJ = FDB(C_b - C_s) \tag{7}$$

The flow velocity profiles near biofilms can also be approximated by an exponential function of velocity versus distance (eq 3). The form of this function is the same as in the case of the substrate concentration profile:

$$\left(\frac{dv}{dX}\right)_{X=0} = Av_b \tag{8}$$

from which the shear stress at the biofilm surface (τ) can be directly calculated as

$$\tau = \mu A v_b \tag{9}$$

where μ is viscosity.

These results may be cautiously compared to a more simple situation: convective transport in the laminar boundary layer over a flat plate (Sissom and Pitts, 1972), for example. The Schmidt number $Sc \equiv \nu/D$ for O_2 diffusing in flowing water is 558 (Bennett and Myers, 1974). Both of the constants (A and B) in the empirical equations for the velocity and concentration profiles have the dimensions of inverse length. If we use extracted parameters as measures of boundary layer thickness, i.e., $1/A$ as a measure of δ_c (the concentration boundary layer thickness) and $1/B$ as a measure of δ (the hydrodynamic boundary layer thickness), we find that $\delta/\delta_c \approx 8$. Sissom and Pitts (1972) give $\delta/\delta_c = Sc^{1/3}$, which is approximately 8.3.

The solutions obtained involved certain assumptions, however. The experiments presented stress the importance of the conditions at and near biofilm surfaces. The biofilm/water interface is a layer of variable thickness rather than a precisely defined plane (Lewandowski et al., 1990). In extreme cases when the biofilm surface is colonized with filamentous microorganisms, the position of the surface can even be a function of flow velocity. The higher the flow velocity the more the filaments will yield to the flow and smooth the surface, resulting in a change in the biofilm boundary. Because the biofilm/water interface is not a clearly defined concept, problems arise when such an interface is treated using existing models of diffusion and hydrodynamics.

When evaluating the flow velocity profiles near a biofilm surface, the position of the surface is assumed to be at the location where velocity reaches zero. This, however, requires the additional assumption that the flow of water is restricted to the volume above the film and does not enter the film. Any experimental measurement also imposes uncertainty on the location of the interface. In this work, the velocity profiles from NMR are summed over a layer of an approximately 3-mm thickness. Thus, the curvature of the biofilm surface can influence the results.

NMR is inherently a low signal to noise (S/N) technique; in order to achieve reasonable S/N in NMR images, spatial and temporal averaging are required. Two types of spatial averaging should be distinguished: in-plane and through-plane. In-plane resolution in the read-out direction is determined by the strength of the read-out gradient and the sampling parameters. In the phase-encoding direction, resolution is determined by the maximum intensity of G_{pe}

and the number of phase-encoding steps N_{pe}. In these experiments, in-plane resolution was approximately 0.1 mm. Through-plane resolution, however, is determined by the thickness of the slice. In these experiments, the minimum slice thickness achieved was 2.5 mm. In the cross-sectional velocity measurements the slice was transverse to the long dimension of the model, and thus our resolution along the streamwise direction was comparable to the channel height (2 mm). In the dual-echo experiments, the slice contained the whole model; thus the velocity components measured were averages of the velocity over the channel height.

The long times required for NMRI data acquisition result in temporal averaging of flow conditions. The steady flow system used in these experiments was periodically monitored by timed collection; flow was steady to within our measurement error of ±3%.

The two techniques described are not quite compatible. NMRI does not tolerate the presence of metals, and the microelectrode technique is difficult to implement in the absence of metals. The use of NMRI excludes metallic components from reactors. Microelectrode techniques require extensive equipment controlling the sensor movement and data acquisition. A reactor designed to conduct the microelectrode measurements outside the magnet subsequently inserted into the magnet to perform hydrodynamic experiments may work. However, even when such a procedure is successful, it would not be a simultaneous measurement. Other techniques, such as laser Doppler or hot wire anemometry, are also considered as options, although each of them has serious disadvantages with regard to biofilm systems. Their weakness shows up close to the biofilm surface where the filamentous growth exists. Filamentous growth constitutes an optical hindrance for laser Doppler and influences the hot wire anemometry when toughing the probes. Hot wire anemometry is also invasive. Nuclear magnetic resonance imaging seems to deliver the most reliable information on velocity distribution near microbially colonized surfaces.

Conclusions

Two techniques were used to describe conditions near biofilms: the microelectrode technique to measure dissolved oxygen profiles and NMRI to measure flow velocity profiles.

The substrate concentration and flow velocity profiles can be described by the same exponential equations with different exponential coefficients. Conditions at the biofilm surface in terms of flux of substrate and shear stress are linear functions of bulk substrate concentration and bulk average flow velocity, respectively, and empirical coefficients. Analytical interpretation of results is obstructed by the lack of theoretical treatment of flow near biofilm-covered surfaces.

The applied techniques, microelectrode measurements of dissolved oxygen concentration and nuclear magnetic resonance imaging of flow velocity distribution, have been proven useful in describing conditions near biofilms despite some limitations.

Acknowledgment

The authors acknowledge support from the Center for Interfacial Microbial Process Engineering at Montana State University, a National Science Foundation-sponsored engineering research center, and the center's industrial associates.

Literature Cited

Abragam, A. *The Principles of Nuclear Magnetism*; Clarendon: Oxford, 1961.

Altobelli, S. A.; Givler, R. C.; Fukushima, E. Velocity and concentration measurements of suspensions by nuclear magnetic resonance imaging. *J. Rheol.* **1991**, *35* (5), 721–734.

Baumgartl, H. Systematic Investigations of Needle Electrode Properties in Polarographic Measurements of Local Tissue PO2. In *Clinical Oxygen Pressure Measurement*; Ehrly, A. M., Hauss, J., Huch, R., Eds.; Springer: Berlin, 1987; pp 17–42.

Bennett, C. O.; Myers, J. E. *Momentum, Heat, and Mass Transfer*; McGraw-Hill: New York, 1974; Table A-19, p 788.

Bouwer, E. J. Theoretical Investigation of Particle Deposition in Biofilm Systems. *Water Res.* **1987**, *21*, 1489–1498.

Bungay, H. R., III; Whalen, W. J.; Sanders, W. M. Microprobe Techniques for Determining Diffusivities and Respiration Rates in Microbial Slime Systems. *Biotechnol. Bioeng.* **1969**, *22*, 765–772.

Caprihan, A.; Fukushima, E. Flow Measurement by NMR. *Phys. Rep.* **1990**, *198*, 195–235.

Cho, Z. H.; Oh, C. H.; Mun, C. W.; Kim, Y. S. Some Results of High Flow-Velocity NMR Imaging Using Selection Gradient. *Magn. Reson. Med.* **1986**, *3*, 857–862.

Cunningham, A. B. Hydrodynamics and Solute Transport at the Fluid-Biofilm Interface. *Structure and Function of Biofilms*; Characklis, W. G., Wilderer, P. A., Eds.; John Wiley: 1989; pp 19–31.

Duddridge, J. E.; Kent, C. A.; Laws, J. F. Effect of Surface Shear Stress on the Attachment of *Pseudomonas fluorescens* to Stainless Steel under Defined Flow Conditions. *Biotechnol. Bioeng.* **1982**, *26*, 153–164.

Fukushima, E.; Roeder, S. B. W. *Experimental Pulse NMR*; Addison-Wesley: Reading, MA, 1981.

Levich, V. G. *Physicochemical Hydrodynamics*; Prentice-Hall, Inc.: Englewood, NJ, 1962; p 57.

Lewandowski, Z.; Walser, G. Influence of Hydrodynamics on Biofilm Accumulation. *Environmental Engineering Proceedings*, EE Div/ASCE, Reno, NV, July 8–10, 1991, pp 619–624.

Lewandowski, Z.; Walser, G.; Larsen, R.; Peyton, B.; Characklis, W. G. Biofilm Surface Positioning. *Environmental Engineering Proceedings*, EE Div/ASCE, Arlington, VA, July 8–11, 1990.

Lewandowski, Z.; Walser, G.; Characklis, W. G. Reaction Kinetics in Biofilms. *Biotechnol. Bioeng.* **1991**, *38*, 877–882.

Lewandowski, Z.; Altobelli, S. A.; Majors, P. D.; Fukushima, E. NMR Imaging of Hydrodynamics near Microbially Colonized Surfaces. *Water Sci. Technol.* **1992**, *26*, 577–584.

Majors, P. D.; Givler, R. C.; Fukushima, E. Velocity and Concentration Measurements in Multiphase Flows by NMR. *J. Magn. Reson.* **1989**, *85*, 235–243.

Majors, P. D.; Caprihan, A.; Fukushima, E. Dual echo flow NMR imaging. In *Proc. 31st Exp. NMR Conf.* Asilomar, CA; ENC: Santa Fe, NM, 1990.

Morris, P. G. *Nuclear Magnetic Resonance Imaging in Medicine and Biology*; Clarendon: Oxford, 1986.

Picologlou, B. F.; Zelver, N.; Characklis, W. G. Biofilm Growth and Hydraulic Performance. *Hydraul. Div., Am. Soc. Civ. Eng.* **1980**, *106*, 733–746.

Revsbech, N. P.; Jorgensen, B. B. Microelectrodes: Their Use in Microbial Ecology. *Advances in Microbial Ecology*; Marshall, K. C., Ed.; Plenum Publishing Corporation: New York, 1986.

Riethues, M.; Buchholtz, R.; Onken, O.; Baumgartl, H.; Lubbers, D. W. Determination of Oxygen Transfer from Single Air Bubbles to Liquids by Oxygen Microelectrodes. *Chem. Eng. Process.* **1986**, *20*, 332–337.

Rittmann, B. E. The Effect of Shear Stress on Biofilm Loss Rate. *Biotechnol. Bioeng.* **1982**, *24*, 501–506.

Siegrist, H.; Gujer, W. Mass Transfer Mechanism in a Heterotrophic Biofilm. *Water Res.* **1985**, *19*, 1369–1378.

Sissom, L. E.; Pitts, D. R. *Elements of Transport Phenomena*; McGraw-Hill: New York, 1972; Chapter 14.

Whalen, W. J.; Bungay, H. R., III; Sanders, W. M., III Microelectrode Determination of Oxygen Profiles in Microbial Slime Systems. *Environ. Sci. Technol.* **1969**, *3*, 2297–2298.

Accepted November 10, 1992.